Catal Surv Asia (2009) 13:164–183
DOI 10.1007/s10563-009-9074-8

Development of Carbon Materials for Energy and Environmental Applications

B. Viswanathan · P. Indra Neel · T. K. Varadarajan

Published online: 8 August 2009

Abstract Methodologies for generating carbon materials from unusual natural sources like *Limonea acidissima* and *Calotropis gigantea* are reported. The carbon materials thus obtained have been characterized using a variety of tools. The possibility of modulating the textural properties of these materials has been examined. The carbon materials synthesized have been exploited for specific applications, such as support for noble metals for use in Direct Methanol Fuel Cells and as support for heteropoly acid for the production of gasoline additive. In addition, the utility of some of the activated carbon materials (from commercial sources) for the removal of sulphur from crude petroleum sources is also examined.

Keywords Carbon materials · Carbon support · Direct methanol fuel cell · TAME · Adsorption of sulfur compounds

1 Introduction

Materials based on carbon have been evolving all the time. In recent times these materials have given rise to a variety of intriguing possibilities in terms of structure, morphology, texture, properties and applications. However, one of the challenging and desired aspects for carbon materials is to find ways of producing these materials from alternate (natural) sources and to tune the textural, structural and surface properties in accordance with the application. This review reports the work carried out by the authors on the preparation of carbon materials from plant sources and the use of different carbons (natural and commercial) in catalysis and adsorption.

B. Viswanathan (✉) · P. I. Neel · T. K. Varadarajan
National Centre for Catalysis Research, Department of Chemistry, Indian Institute of Technology, Madras, Chennai 600036, India
e-mail: bvnathan@iitm.ac.in

2 Carbon Material from *Limonea acidissima* Shells for Electrocatalytic Applications

Activated carbon materials from natural sources (lignocellulosic materials) have been widely exploited for sorption and catalytic applications. Such materials have remained unexplored for energy conversion device applications. Activated carbon material was synthesized from *Limonea acidissima* (wood apple) shells using KOH as activating agent. The carbon material (C_{WA}, Carbon from wood apple shell) obtained was used as support for Pt. The electrocatalyst Pt/C_{WA} was employed for the fabrication of anode for the electroxidation of MeOH [1].

3 Fuel Cells as Clean Energy Sources

In a fuel cell, the chemical energy of the fuel is directly converted to the electrical energy through a chemical reaction [2]. Electric current can be generated by the direct electrochemical oxidation of MeOH. The electroxidation reaction of methanol at the anode can be represented as follows [3]:

$$CH_3OH + H_2O \rightarrow CO_2 + 6H^+ + 6e^- \quad E^0 = 0.02\,V$$

The reaction of MeOH electrooxidation bears technological significance in the operation and exploitation of Direct Methanol Fuel Cells. DMFCs hold promise as a clean energy source for future transportation demands.

Typical stationary and mobile applications of fuel cells include electrification of residences, providing power to mobile phones, lap top computers and other portable electronic devices [4].

4 Challenges in the Development of Fuel Cell Anode Electrocatalyts

Platinum group metals (PGM's) are most widely used for electrode applications. There are two major problems associated with the development of DMFC. The first is poisoning of the electrode by CO [5]. Phosphoric acid fuel cells can withstand upto 2% CO in the fuel stream. But Proton exchange membrane fuel cells can only withstand ppm levels of CO. The second problem is the high cost of the catalyst restricting the rapid and wide spread commercialization of fuel cells. There are two approaches by which one can solve the above two problems. One approach is to find suitable alternatives (partial or complete) to the active component i.e., Pt and the second approach is to find suitable alternative to Vulcan XC 72 R carbon black which is the best carbon support material commercially used till date [6]. For example, Samant et al. [7] have generated a catalyst more active than 10 wt% Pt/Vulcan XC 72 R just by changing the support i.e., by replacing Vulcan XC 72 R with mesoporous carbon produced by a sol-gel method.

In general, high specific surface area carbon material is employed as support for Pt for fuel cell electrode applications. The carbon support facilitates the dispersion of the stable metal crystallites with favourable electronic and metal support interaction [8]. The carbon support influences the electrochemical properties and in turn the performance of Pt-based electrocatalysts. The nature of carbon material (oxygen surface functional groups, electronic conductivity, pore structure, morphology, electrochemically accessible surface area) determine the electrochemical performance of electrode catalysts. Electronic conductivity, surface area (electro active as well as BET), porosity, micro structure, macro morphology, corrosion resistance and cost are some of the important properties that determine the suitability of a carbon material for electrode applications.

Any breakthrough in the commercialization of DMFC's is possible only by significant improvements either in the replacement of *active Pt metal* or *the support carbon material*.

5 Carbon Material from *Limonea acidissima* Shell by KOH Activation

Limonea acidissima (Wood Apple) shells were conceived for the first time as a source for activated carbon. The fruit,

Fig. 1 Wood apple (*Limonea acidissima*) fruits

Limonea acidissima (Fig. 1) is native to India and other Asian countries. *Limonea acidissima* is also called as *Feronia elephantum*, *Feronia limonia*, *Hesperethusa crenulata*, *Schinus limonia*, Wood apple, Elephant apple and Curd fruit. The shells of *Limonea acidissima* (wood apple) have features bearing close resemblance to that of coconut shells. Activated carbon from *Limonea acidissima* is produced by the chemical activation method using KOH as activating agent.

5.1 Method of Synthesis of Carbon Material

Typical method of synthesis of carbon material involves the soaking of a known amount (50 g) of dried shells of *Limonea acidissima* in 100 mL of 50 wt% *KOH* solution for 2 h. Excess KOH solution is then decanted. The shells soaked in KOH solution are then dried in an air oven at 150 °C followed by subjecting the same to thermochemical activation in a N_2 atmosphere at 800 °C for 2 h. The char thus obtained is subsequently treated with conc. HNO_3. The char to conc. HNO_3 ratio (wt/wt%) is 1:5.

5.2 Characterization of Carbon Material from *Limonea acidissima*

5.2.1 BET Sorptometry—Textural properties of Carbon Material

N_2 adsorption–desorption isotherms obtained for the activated carbon from *Limonea acidissima* are shown in Fig. 2. The corresponding pore size distribution curve (BJH) is also shown in the insert of the figure. The isotherm in Fig. 2 is of type I, characteristic of a microporous material. The pore size distribution reveals the pore dimensions to be less than 2 nm suggesting that the activated carbon material is micorporous in nature.

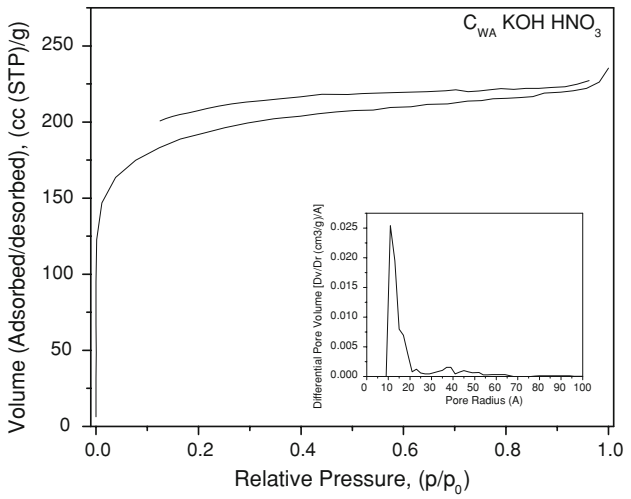

Fig. 2 N_2 adsorption-desorption isotherm of carbon material prepared from *Limonea acidissima*; the corresponding pore size distribution of the activated carbon material is shown in the insert; $S_{BET} = 698\ m^2/g$; Pore volume (V_p) = 0.35 cm^3/g; and Mean pore diameter = 2.0 nm

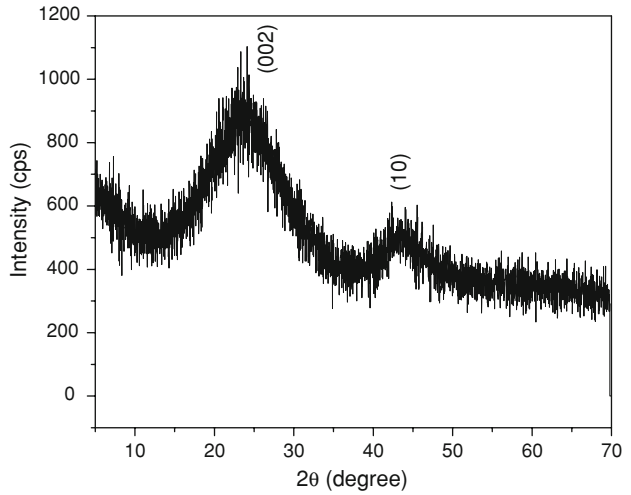

Fig. 3 XRD pattern of carbon material prepared from *Limonea acidissima* shells by KOH activation method

5.2.2 XRD Studies—Structural (Crystal) Details of Carbon Materials

The X-ray diffraction pattern obtained for the activated carbon material from *Limonea acidissima* shells is shown in Fig. 3. Two broad diffraction peaks centered around 2θ values of 24 and 43° which are, respectively, attributed to the reflections from the (002) and (10) planes (the (hk) line is because of intra layer scattering) of the carbon material. The values of average crystallite sizes along the c-axis (stacking axis) and the a-axis were determined using the Debye–Scherrer equation. Shape factor, k, values of 0.89 and 1.84 were employed for the calculation of values of L_c and L_a respectively. The diffraction angles as well as the value of full width at half maximum corresponding to the diffraction planes of (002) and (10) were employed for the calculation of values of L_c and L_a respectively. The values of L_c and L_a were found to be of the order of 1.1 and 3.656 nm respectively. The values of L_c and L_a for typical graphitic carbon structure are 0.0670 and 0.2461 nm respectively [9, 10]. The magnitude of the values of L_c and L_a of the activated carbon materials from *Limonea acidissima* (obtained by KOH activation) indicate that the carbon material contained roughly about 16 cell lengths along the c-direction and nearly 15 cell lengths along the a-direction.

5.2.3 Confocal Raman Spectroscopic Studies—Structural (Crystal, Order, Disorder, Defect) Details of Carbon Materials

Details of structural disorder as well as the crystallographic parameter of the activated carbon material produced by KOH activation of the shells of *Limonea acidissima* were obtained from the Confocal Raman spectrum shown in Fig. 4. Two characteristic Raman peaks centered around 1,348 and 1,591 cm^{-1} were observed in the confocal Raman spectrum. These two bands were designated as D (disordered) and G (graphitic) bands and were attributed to the A_{1g} and E_{2g} Raman active C–C vibration modes with in the graphitic layer. The Raman peaks at 1,348 and 1,591 cm^{-1} are called the first order Raman peaks. The other details deduced from the Raman spectrum are: $R(I_D/I_G) = 1.408$; $L_a = 4.4/R = 3.125$ nm. This value is comparable to the value of L_a deduced from XRD pattern (3.656 nm).

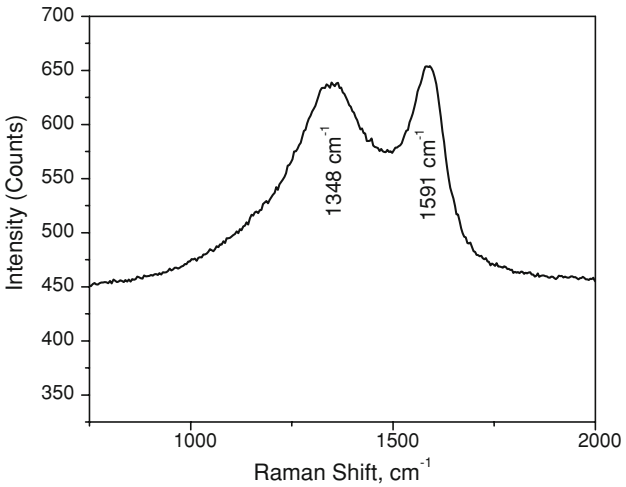

Fig. 4 Confocal Raman spectrum of activated carbon produced from *Limonea acidissima* by KOH activation

The Raman intensity ratio (the ratio of the integrated intensities of the D and G bands) (I_D/I_G) is a measure of the extent of disorder with in a carbon layer. The R value for the activated carbon material from *Limonea acidissima* was found to be 1.408 which is typical of disordered carbon materials like glassy carbon. The slight variation (≈ 5 Å) in the L_a value obtained between Confocal Raman spectrum and X-ray diffraction pattern is attributed to the ±7% error involved in the calculation of the integrated intensity values under the D band and G band. Since line width from XRD is more accurately determined compared to the integrated intensity values under the D and G bands in the confocal Raman spectrum, the L_a value obtained from wide angle X-ray studies is more reliable.

5.2.4 *Electron Paramagnetic Resonance Spectroscopic Studies—Dangling Bond Concentration*

The electron paramagnetic resonance (EPR) spectrum of activated carbon from *Limonea acidissima* is shown in Fig. 5. The EPR spectrum was recorded on a X-band EPR spectrometer operating at a microwave frequency of 9.2 GHz at room temperature using diphenyl picryl hydrazyl radical as the external reference. The g value of the resonance signal for the activated carbon is 2.03095 which is close to the free electron g-value.

The origin of the EPR signal is attributed to the presence of dangling bonds in the carbon structure. The concentration of unpaired spins was found to be 1.3×10^{18} spins/g of the carbon material. The spin concentration value of activated carbon from the stems of *Limonea acidissima* (C_{WA}) is an order of magnitude lower than that of the spin concentration values reported for commercial acetylene

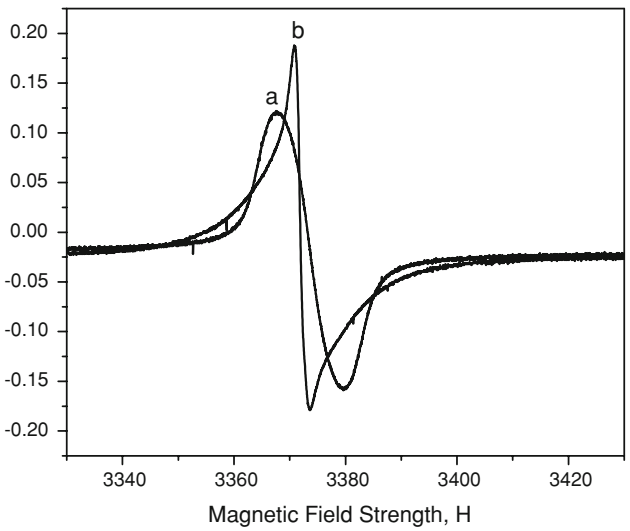

Fig. 5 EPR spectrum of activated carbon from *a Limonea acidissima* by KOH activation and *b* DPPH (reference)

based carbon (3.8×10^{19}) and graphon (1.1×10^{19}) [30]. The lower spin concentration in our sample is because of the saturation of the dangling bonds with potassium, formed during the carbothermal reduction of K_2CO_3, resulting in the formation of surface C–K bonds which subsequently transform (partially) to C–H bonds upon final treatment with conc. HNO_3. The formation of C–K type bonds is also confirmed from the presence of 0.45 wt% K in the activated carbon material even after treatment with conc. HNO_3 (Fig. 6). The transformation is also confirmed from the appearance of C–H bonds in the FT-IR spectrum shown in Fig. 7.

5.2.5 *Scanning Electron Microscopy and Energy Dispersive X-ray Analysis—Morphology and Elemental Composition*

Details of the surface morphology as well as the elemental composition of the activated carbon material were obtained using High resolution scanning electron microscopy (HR SEM, FEL, Model: Quanta 200) equipped with Energy dispersive X-ray analysis facility. Scanning electron microscope images are obtained at a magnification of 4,000× and 10,000× and at a scanning voltage of 30 kV. A highly heterogeneous and rough surface with a continuous porous net work is viewed on the surface of the activated carbon produced from *Limonea acidissima*. The porous network is clearly viewed at the higher magnification (10,000×) (Fig. 6a, b).

The chemical composition of the activated carbon material was determined using energy dispersive X-ray analysis. A high carbon content of 74.84 wt% was found. In spite of treatment with HNO_3, 0.45 wt% K was inevitably present in the activated carbon. The oxygen content was found to be 24.7 wt% (19.83 atomic %).

5.2.6 *FT-IR Spectroscopic Studies—Surface Functional Groups*

Fourier transform infrared (FT-IR) spectroscopy provides evidence for the presence of specific functional groups on the surface. The FT-IR spectrum of activated carbon from *Limonea acidissima*, C_{WA}, was recorded on Shimadzu spectrophotometer. The spectral range of analysis is 450–4,000 cm^{-1} with a resolution of 4 cm^{-1}. The spectrum was obtained in transmission mode at 20 scans. Pressed KBr pellets were prepared by grinding 200 mg of carbon samples with 0.5 g of KBr. Several characteristic bands were observed in the FT-IR spectrum shown in Fig. 7 and each of the bands has been assigned to specific functional group based on the assignments reported in literature.

Even though a cluster of functional groups are present on the carbon surface, the prominent among them are: a

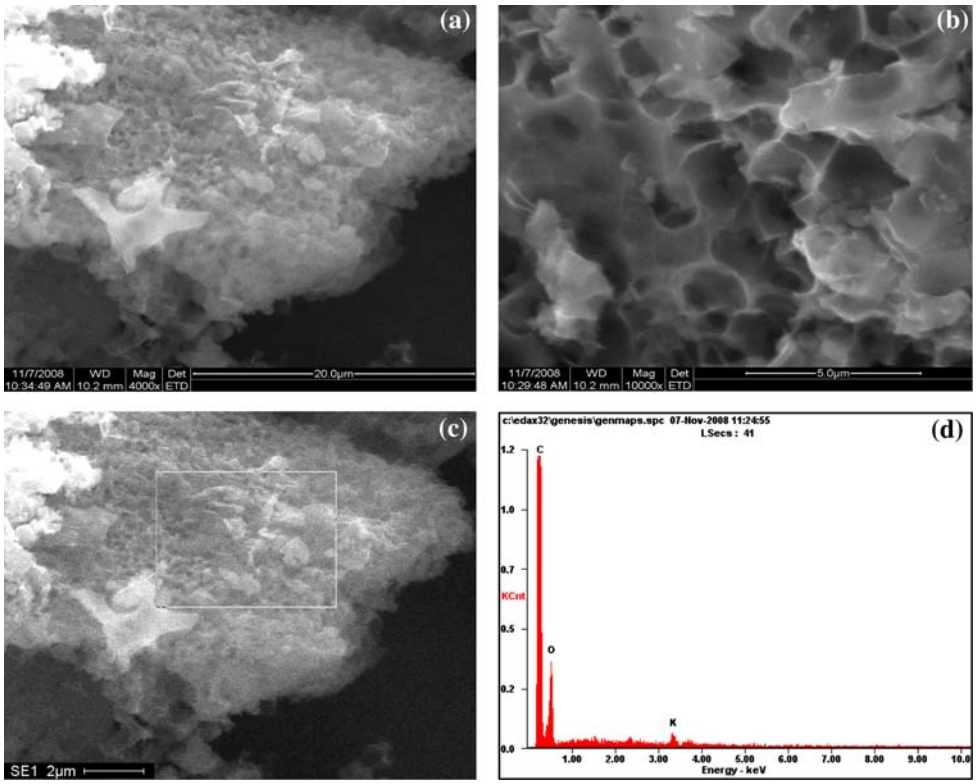

Fig. 6 SEM images and EDAX spectrum from the activated carbon material from *Limonea acidissima* using KOH activation; at a magnification of **a** 4,000×, **b** 10,000×, **c** selected region for elemental analysis and **d** energy dispersive X-ray analysis spectrum

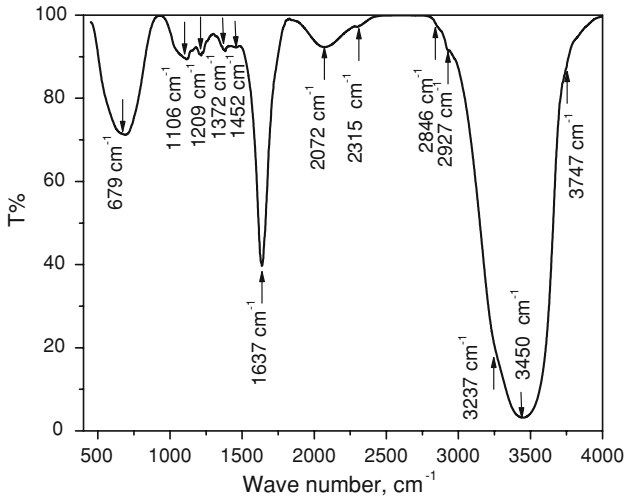

Fig. 7 FT-IR spectrum of activated carbon produced from *Limonea acidissima* shells using KOH activation

sharp and intense band centered around 1,637^{-1}, which is attributed to the carbonyl (C=O) stretching vibration of quinone. The carbon surface is oxidized by treatment with conc. HNO_3 leading to the generation of such quinone type carbon functional groups, which bear significance in the redox chemistry of carbon materials. Such carbonyl functional groups are known to be pronounced in the case of oxidized carbon materials rather than the original parent carbon material. In addition, a broad and intense band is observed in the range of 3,200–3,600 cm^{-1}, centered at 3,450 cm^{-1} attributable to the O–H stretching vibration of surface hydroxylic groups as well as to the adsorbed water. The asymmetry of this band (a shoulder at a lower wave number, 3,237 cm^{-1}) indicates the presence of strong hydrogen bonding interactions.

6 Fabrication of Anode Electrocatalyst for DMFC Application with the Carbon Material Obtained from *Limonea ascidissima* Shell

Lack of efficient and inexpensive electrocatalysts for MeOH oxidation is a challenge for the large scale utility of direct methanol fuel cells. The objective of this work is to design a cost effective and highly active electrocatalyst by developing new porous carbon material as support for Pt, as alternative to Vulcan XC 72 R.

6.1 Preparation of Pt/C Catalysts

Pt supported carbon catalysts have been prepared by impregnating hexachloroplatinic acid in carbon material followed by reduction of Pt (4+) to Pt (0) in hydrogen atmosphere at 450 °C for 2 h. Catalysts with different wt% loadings, namely, 5, 10 and 20 wt%, of active component

(Pt) on the carbon support (C_{WA}) were prepared by adding the requisite amounts of a H_2PtCl_6 solution to the carbon support (C_{WA}) and drying at 110 °C. A 20 wt% Pt/Vulcan XC 72 R prepared under identical conditions was employed as a reference for comparing the performance of C_{WA} carbon material relative to that of Vulcan XC 72 R carbon black.

6.1.1 XRD Analysis of Pt/C Catalysts

The X-ray diffractograms of 5, 10, and 20 wt% Pt on carbon material obtained from the shells of *Limonea acidissima* (wood apple) are shown in Fig. 8. For comparison the XRD pattern of 20 wt% Pt/Vulcan XC 72 R is also shown in Fig. 8. Diffraction peaks characteristic of Pt metal with a face centered cubic lattice are observed and the peaks are all indexed as (111), (200), (220), (311) and (222) (JCPDS file No. 87-0647). The crystallite size of Pt calculated using Debye-Scherrer equation [11] and the lattice parameter values of Pt metal in the case of each of the catalysts (Pt/C_{WA} and Pt/Vulcan XC 72 R) was calculated. The broad diffraction peak centered around a 2θ value of 24° corresponds to the (002) reflection of the carbon support with a turbostratic graphitic structure. The lattice constant value of ~0.39 nm correlates well with the FCC lattice of Pt metal supported on carbon materials [JCPDS file No. 87-0647]. The lattice constant value of Pt metal is (0.3923 nm) [12].

Reflection from the (220) plane of Pt metal was used for the calculation of the crystallite size as it is away from the region of the broad diffraction peak (from (002) plane) of the carbon support. The crystallite size of Pt is found to be dependent on the Pt loading and also on the nature of the carbon support. With the same amount of Pt loading (20 wt%), the crystallite size of Pt on carbon produced from *Limonea acidissima* shell is smaller (10.4 nm) than on Vulcan XC 72 R (13.1 nm) indicating better dispersion of Pt on the C_{WA} support due to the enhanced surface oxygen functional groups as well as the higher value of specific surface area. Also, the Pt crystallite size was found to be the least (5 nm) in the case of 5 wt% Pt/C_{WA}.

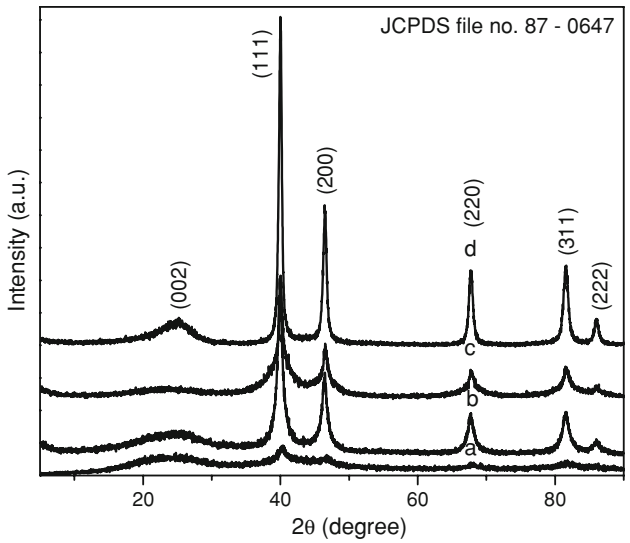

Fig. 8 X-ray diffraction patterns of *a* 5 wt% Pt/CWA (crystallite size ~5.0 nm) *b* 10 wt% Pt/CWA (crystallite size ~10.2 nm) *c* 20 wt% Pt/CWA) (crystallite size ~10.4 nm) and *d* 20 wt% Pt/Vulcan XC 72 R (crystallite size ~13.1 nm)

6.1.2 BET Sorptometric Studies—Textural Properties of the Pt/C Catalysts

The textural properties of the Pt/C_{WA} catalysts were investigated by BET sorptometry. At all loadings the Pt/C_{WA} catalysts exhibited typical type I isotherms (not shown) characteristic of microporous solids. An important observation was that the surface area and the volume of N_2 (adsorbate) adsorbed decreased drastically as the wt% loading of Pt increased (5 wt% Pt/C_{WA} [$S_{BET} = 505\ m^2/g$, $V_p = 0.289\ cm/g$], 10 wt% Pt/C_{WA} [$S_{BET} = 526\ m^2/g$, $V_p = 0.288\ cm^3/g$] and 20 wt% Pt/C_{WA} [$S_{BET} = 195\ m^2/g$, $V_p = 0.115\ cm^3/g$]. For comparison the textural properties of 20 wt% Pt/Vulcan XC 72 R catalyst are: ($S_{BET} = 123\ m^2/g$, $V_p = 0.294\ cm^3/g$).

7 Evaluation of Electrocatalytic Activity of Pt/C Catalysts

7.1 Electroxodiation of MeOH—Cyclic Voltammetry

Cyclic voltammetric studies were carried out on a BAS Epsilon potentiostat using modified glassy carbon (Bioanalytical system, USA) as the working electrode, Ag/AgCl (saturated KCl) as the reference electrode and a platinum foil (1.5 cm^2) as an auxiliary electrode. 0.5 M H_2SO_4 was employed as supporting electrolyte. The electrochemical measurements were carried out in a conventional three-electrode glass cell. The MeOH oxidation reaction was carried out with 1 M CH_3OH in acid medium.

The cyclic voltammograms recorded with electrodes fabricated using 5, 10 and 20 wt% Pt supported on carbon material C_{WA} are shown in Fig. 9. For comparison, the cyclic voltammetric response from the electrode fabricated with 20 wt% Pt supported on Vulcan XC 72 R is also shown in Fig. 9. The feature common to all the cyclic voltammograms is that one anodic peak is observed in the forward scan and another in the reverse scan. The anodic peak in the forward scan is attributed to oxidation of MeOH [13–18]. The anodic peak in the reverse scan is attributed to the removal of the incompletely oxidized

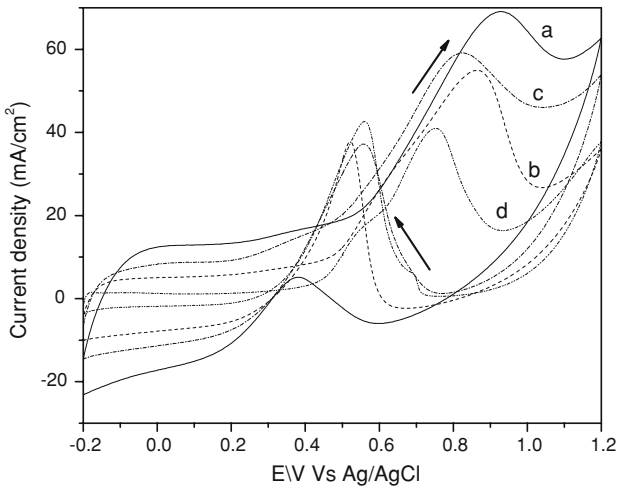

Fig. 9 Cyclic voltammetric response of *a* GC/C_{WA}—5 wt% Pt-Nafion electrode; *b* GC/C_{WA}—10 wt% Pt-Nafion electrode; *c* GC/C_{WA}—20 wt% Pt-Nafion electrode; and *d* GC/Vulcan XC 72 R—20 wt% Pt-Nafion electrode in 0.5 M H_2SO_4 and 1 M MeOH, at a scan rate of 25 mV/s between −0.2 and 1.2 V versus Ag/AgCl

carbonaceous species (mostly in the form of linearly bonded Pt=C=O) formed in the forward scan [13].

The critical parameter that determines the usefulness of an electrode is the onset potential. A less positive value of the onset potential is preferred. A lower onset (less positive potential) potential value implies the requirement of lower energy of the MeOH oxidation reaction to take place [19]. The onset potential value is related to the breaking of the C-H bond of MeOH which is the primary step involved in the mechanism of electroxidation of MeOH [20]. The onset potential values for the electroxidation of MeOH deduced from the cyclic voltammograms obtained over different electrodes, along with peak potential and current values corresponding to the MeOH oxidation (anodic peak in the forward sweep) as well as the oxidation of the intermediate species formed during the oxidation of MeOH (anodic peak in the reverse sweep) are summarized in Table 1. Zhaoling Liu et al. [21] have reported the onset potential vaues of 0.27 and 0.28 V, respectively, on Pt/Vulcan XC 72 R and Pt/CNT's for the electrooxidation of MeOH in 1 M H_2SO_4 and 2 M MeOH at a scan rate of 50 mV/s.

The onset potential being a little lower (0.21 V) than the commercial vulcan carbon (0.25 V), 5 wt% Pt/C_{WA} showed a higher current density which is an indication of higher electrochemical catalytic activity. Such high current values derivable from the modest wt% loadings of Pt is an indication of the effective utilization of Pt over the C_{WA} support. The improved performance of the electrocatalyst, 5 wt% Pt/C_{WA}, is attributed to the high electro catalytic activity of the Pt nano crystallites (5.0 nm) finely dispersed over the carbon support.

The ratio of the anodic peak current densities in the forward (i_f) and reverse (i_b) scans too gives a measure of the catalytic performance. A higher i_f/i_b ratio indicates superior oxidation activity of methanol during the anodic scan and less accumulation of carbonaceous species on the nanocatalyst surface and thus an indication of better CO tolerance. The i_f/i_b value in the case of 5 wt% Pt/C_{WA} catalyst is 14.4 which is an order of magnitude higher than that of either 20 wt% Pt/C_{WA} or 20 wt% Pt/Vulcan XC 72. The i_f/i_b value of the electrocatalyst produced from commercial fuel cell grade Vulcan XC 72 carbon was found to be 0.96. At all the loadings of Pt, the electrodes fabricated using C_{WA} carbon materials showed an i_f/i_b value greater than 0.96 (value obtained for Vulcan XC 72 R based catalyst). For comparison, the i_f/i_b value for 20 wt% PtRu/C catalyst of commercial Johnson Matthey sample is 1.33 [22].

7.2 MeOH Electrooxidation—Evaluation of Stability of the Electrode-Chronoamperometry

The long term stability of the fabricated electrodes was evaluated by chronoamperometric studies carried out for a duration of 3 h with the electrode being polarized at +0.6 V versus Ag/AgCl in 0.5 M H_2SO_4 and 1 M MeOH. The initial and final (after 3 h) current density values

Table 1 Effect of Pt loading and the nature of the carbon support on the electro catalytic activity of MeOH Electrooxidation of Pt/C_{WA} and Pt/Vulcan XC 72 R

S. no.	Electrode	Onset potential, *V*	i_f/i_b	Activity[a]			
				Forward sweep		Reverse sweep	
				I (mA/cm^2)	*E* (V)	*I* (mA/cm^2)	*E* (V)
1	GC/C_{WA}-5% Pt-Nafion	0.21	14.4	69.0	0.92	4.97	0.37
2	GC/C_{WA}-10% Pt-Nafion	0.18	1.45	55.0	0.86	37.6	0.52
3	GC/C_{WA}-20% Pt-Nafion	0.18	1.60	58.9	0.82	37.28	0.51
4	GC/Vulcan XC 72 R-20% Pt-Nafion	0.25	0.96	40.9	0.75	42.6	0.56

[a] Activity evaluated in 0.5 M H_2SO_4 and 1 M MeOH, at a scan rate of 25 mV/s between −0.2 to 1.2 V versus Ag/AgCl

Table 2 Evaluation of the stability of C_{WA} based electrodes for the electrooxidation of MeOH in half cell mode

S. no.	Electrode	Activity[a]		% Decrease in activity after 3 h at +0.6 V
		Initial (I), [$mAcm^{-2}$]	Final (I), [$mAcm^{-2}$]	
1	GC/C_{WA}-5% Pt-Nafion	25.2	19.1	24
2	GC/C_{WA}-10% Pt-Nafion	29.7	19.0	36
3	GC/C_{WA}-20% Pt-Nafion	36.1	3.7	89

[a] Activity evaluated in 0.5 M H_2SO_4 and 1 M CH_3OH for 3 h with the electrode being polarized at +0.6 V versus Ag/AgCl

derivable from the electrodes fabricated from 5, 10 and 20 wt% Pt/C_{WA} electocatalysts are summarized in Table 2. The percentage decrease of the activity of the aforementioned electrodes after 3 h is also shown in Table 2. Among the electrodes studied, the 20 wt% Pt/C_{WA} catalyst based electrode showed least stability with a 89 percentage decrease of initial activity at the end of 3 h. In sharp contrast, as expected, the electrode fabricated using 5 wt% Pt/C_{WA} possessing the smallest Pt crystallites (5.0 nm) as well as high i_f/i_b ratio showed highest stability. Only 24% loss in the initial activity is observed at the end of 3 h in the case of the GC/C_{WA}—5% Pt-Nafion electrode. Thus, it is clear that the stability of the electrode is based on the smaller crystallite size of Pt as well as the high CO tolerance (high i_f/i_b ratio value).

The activated carbon material produced from *Limonea acidissima* by KOH activation is a promising support for Pt for the electroxidation of MeOH. The excellent performance of 5 wt% Pt/C_{WA} is attributed to the increase in the extent of utilization of Pt metal. Thus the use of carbon material from *Limonea acidissima* as support for Pt offers the promise of effective utilization of Pt, high electrooxidation (MeOH) activity, high CO tolerance and long term stability. A strong correlation was found between the Pt crystallite size and the electooxidation activity and stability of the carbon supported Pt catalysts.

8 Carbon Material from *Calotropis gigantea* stems for Catalytic Applications

Microporous activated carbon with a large surface area and a narrow pore size distribution has been prepared from the dried stems of *Calotropis gigantea* [23]. *Calotropis gigantea* (Fig. 10) is a waste land weed native of India. Many activating agents, such as $ZnCl_2$, alkali and alkaline earth carbonates, organic acids and their salts have been used activation purposes. The characteristics (textural) of the prepared carbon materials were dependent on the activating agents used and the methodology used. A brief review of the preparation and the characteristics of the carbon materials prepared from the stems of *Calotropis gigantea* is now reported in the following section.

Fig. 10 Stems, leaves and flowers of *Calotropis gigantea*

9 Preparation of Activated Carbon Using $ZnCl_2$ as the Activating Agent

Activated carbon material was produced from *Calotropis gigantea* stems using $ZnCl_2$ as activating agent. Char (as synthesized) was obtained from *Calotropis gigantea* by heating the dried stems of the plant in a muffle furnace at 300 °C [23]. The coal obtained was ground, sieved and treated with Conc. HCl to remove alkali and alkaline metal impurities. The char was further treated with a base (NaOH) to remove siliceous materials The process of activation with $ZnCl_2$ was carried out at 800 °C in N_2 atmosphere for 8 h with varying amounts of activating agent to char (wt/wt%) ratios, namely, 1, 2, 3, 4 and 5. $ZnCl_2$ was added to the char in the solid state by mechanical grinding.

9.1 Characterization of Activated Carbon Produced from $ZnCl_2$ Activation

Textural and structural parameters and properties of the activated carbon materials were found to be influenced by the amount of the activating agent ($ZnCl_2$) as revealed from the Sorptometric, XRD and Confocal Raman studies.

Table 3 Effect of amount of activating agent ($ZnCl_2$) on the textural properties of carbon materials produced from *Calotropis gigantea*

S. no.	Sample	$ZnCl_2$:C (wt/wt%)	S_{BET} (m^2/g)	V_P (cm^3/g)	Mean pore diameter[a] (nm)
1	Char	0	97	0.08	3.3
2	AC1	1	356	0.21	2.36
3	AC2	2	493	0.25	2.03
4	AC3	3	564	0.30	2.13
5	AC4	4	573	0.29	2.02
6	AC5	5	553	0.29	2.1

AC activated carbon

[a] Mean pore diameter, $d = 4\ V/A$ (in nm), where V is the total pore volume and A is the specific surface area

9.1.1 BET Sorptometry—Textural Properties

Irrespective of the amount of the activating agent, all the activated carbon materials presented type I adsorption isotherms for N_2 adsorption at 77 K typical of microporous materials. The specific surface area values, total pore volume as well as the average pore diameter details deduced from the isotherms are summarized in Table 3. The specific surface area values of the carbon materials produced gradually increase (Table 3) with $ZnCl_2$ to char (wt/wt%) ratio upto 4 and beyond which no increase in the S_{BET} value is observed indicating that the optimum value of $ZnCl_2$:Char ratio is 4.

9.1.2 XRD Studies—Crystallographic Structure

The crystallographic parameters of the activated carbon materials produced by $ZnCl_2$ activation of *Calotropis gigantea* were obtained from X-ray diffraction studies.

Three typical broad diffraction peaks centered around 2θ values of 25, 44 and 80° are visible in the activated carbons generated with the activating agent to char impregnation ratios of 1, 2, 3, 4 and 5. The two broad peaks centered around the 2θ values of 25 and 44 are attributed (002) and (10) diffraction peaks of turbostratic carbon structure [24]. The origin of the broad peak around 2θ value of 80° is not yet clearly known. The (00 l) line is because of interlayer scattering where as the (hk) line is because of intra layer scattering. Thus the extent of graphitization is revealed by the appearance of general (hkl) reflections [25–27]. The occurrence of broad diffraction bands centered around 2θ values of 25 and 44 indicates better layer alignment as well as an increased regularity in the crystal structure [28].

The interlayer spacing values, d_{002}, and the crystallite size values along the c (L_c) and a (L_a) axis of the turbostratic graphitic carbon deduced from the X-ray diffractograms are summarized in Table 4. Using the Scherrer equation, the crystallite size along the c-axis, L_c and the size of the large planes, L_a, were determined from the diffraction peaks centered at 2θ values of 25 and 44°.

The interlayer spacing values, d_{002}, almost remained unchanged with impregnation ratio of $ZnCl_2$ to char. The interlayer spacing values, d_{002}, summarized in Table 4 are in the range of 0.35–0.356 nm. These values are greater than 0.335 nm, which is the typical value of the interlayer spacing for pure graphitic carbon. L_c values for different activated carbon materials, summarized in Table 4, are of the order of 1 nm. A decreasing trend in the L_c value is observed with an increase in the amount of the activating agent. The L_c value is the smallest for the activated carbon with the highest S_{BET} value. The L_a values varied in the range of 3.5–3.96 nm. For typical graphitic carbon, the L_c and L_a values are respectively 0.06708 and 0.2461 nm. The magnitude of L_c and L_a values of the activated carbon materials from *Calotropis gigantea* (obtained by $ZnCl_2$ activation) indicate that the carbon material was made up of crystallites with dimensions of (on the average) about 15 cell lengths along the c-direction and about 14–16 cell lengths along the a-direction.

9.1.3 Raman Scattering Studies—Order and Disorder in Carbon Structure

The microstructural changes and the extent of crystallographic disorder (concentration of lattice defects in the graphitic structure) in the activated carbon materials produced from Calotropis gigantia by employing $ZnCl_2$ as

Table 4 Effect of amount of activating agent ($ZnCl_2$) on the structural properties of carbon materials produced from *Calotropis gigantea*

S. no.	Sample	$ZnCl_2$:C (wt/wt%)	d_{002} (nm)	L_c (nm)	L_a (nm)
1	AC1	1	0.356	1.04	3.94
2	AC2	2	0.356	1.02	3.50
3	AC3	3	0.353	1.03	3.96
4	AC4	4	0.356	0.91	3.72
5	AC5	5	0.350	0.94	3.80

AC activated carbon

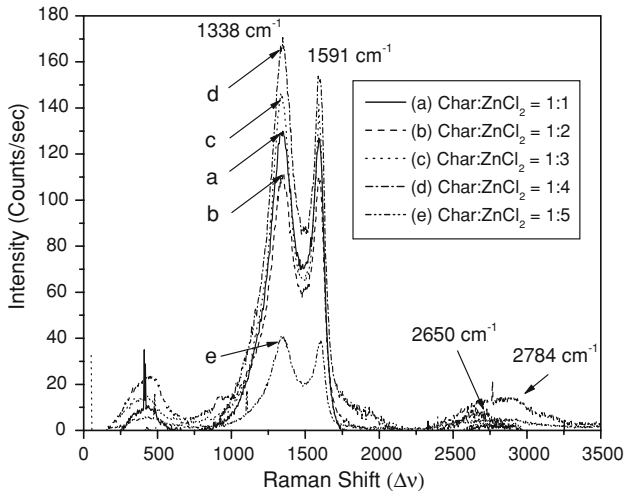

Fig. 11 Confocal Raman spectra of activated carbon materials prepared from *Calotropis gigantea* with a Char to $ZnCl_2$ ratio (wt/wt%) of *a* 1:1, *b* 1:2, *c* 1:3, *d* 1:4 and *e* 1:5

activating agent were analysed using confocal Raman Spectroscopic studies. The Raman spectra, shown in Fig. 11, resulting from activated carbon materials produced by varying the ratios of the activating agent ($ZnCl_2$) to the char (wt/wt%), namely, 1, 2, 3, 4 and 5, were recorded on a Confocal Raman instrument (CRM 200) using Ar ion laser (514.5 nm) as irradiation source.

Irrespective of the amount of the activating agent, all the carbon materials, showed both first order (1,200–1,600 cm^{-1}) and second order (2,400–3,300 cm^{-1}) Raman lines. The information derived from the features of the first and second order Raman lines are important to assess the structural order or disorder in the carbon structure and to find out whether it is amorphous or graphitic. First order Raman lines speak only about the structural order or disorder with in the carbon sheet or layer, ie, carbon plane along *a*-axis. They are silent about the stacking order or disorder in carbon structure. On the contrary, second order lines hold information about the structural (stacking) disorder along the crystallographic *c*-axis [29].

The two first order lines centered around 1,590 (D-band) and 1,348 (G-band) cm^{-1} are attributed to the graphitic and disordered carbon structure. Here the term "graphitic" means carbon atoms which are three coordinated and are bound by sp^2 type bonding orbitals and has nothing to do with the stacking of layers along c-direction. The disorder in the carbon sheet may be because of the non-planar microstructure distortions or because of the disorganized regions near the crystal edges. Lattice defects such as edge dislocation and lattice vacancies too contribute to the band at 1,348 cm^{-1}. Important information extracted from the Raman spectra in Fig. 11 is summarized in Table 5.

The Raman intensity ratio (*R*) which is a measure of the extent of disorder (quantity of defects and vacancies and dislocations) is found to decrease initially upto the activating agent to char impregnation ratio of 3 beyond which it (*R*, disorder) increases. An inverse relation is observed between the value of *R* and the stack width L_a (crystallite size along *a*-axis). The position of the D band (peak intensity position) and the relative intensity of the D band are found to be structure sensitive. An increase in the frequency value of the D band is correlated with a decrease in the crystallite size (L_a) and vice-versa. A strong correlation between the structural parameters deduced from XRD studies (Table 4) as well as Raman studies (Table 5) is observed as the two afore mentioned techniques are mutually complimentary to each other. Interestingly, the L_a values ($L_a = 44/R$ in Å) deduced from the relative intensity of the D band of the activated carbon materials correlates well with the L_a values obtained from XRD studies using the Scherrer equation (Table 4). But, it should be noted that the measurement of line width from the XRD is more accurate than the measurement of the integrated peak intensity values deduced from the Raman spectra. As a result, the L_a values derived from XRD are more reliable than those deduced from the Raman spectra. In addition, the integrated intensity values from Raman spectra are sensitive to the choice of the base line. As a result, the Raman intensity ratio's (*R*) shown in Table 5 are uncertain upto ± 7%.

9.1.4 *Scanning Electron Microscopic Analysis—Details of Surface Morphology*

The SEM image reveals that the carbon material is composed of sheets with well aligned uniform cylindrical pores of diameter (size) 2.4 μm (Fig. 12).

Table 5 Structural parameters (from Raman spectra) of the activated carbon materials from *Calotropis gignatea* activated with $ZnCl_2$

S. no.	Sample	$ZnCl_2$: C (wt/wt%)	Peak intensity frequency, ν_x (cm^{-1})		$R = I_D/I_G$	L_a (nm) = 4.4/*R* (from Raman)	L_a (nm) [from XRD]
			G band	D band			
1	AC1	1	1,591	1,348	1.40	3.14	3.94
2	AC2	2	1,591	1,355	1.42	3.09	3.50
3	AC3	3	1,591	1,331	1.33	3.30	3.96
4	AC4	4	1,587	1,348	1.48	2.97	3.72
5	AC5	5	1,606	1,348	1.53	2.87	3.80

AC activated carbon

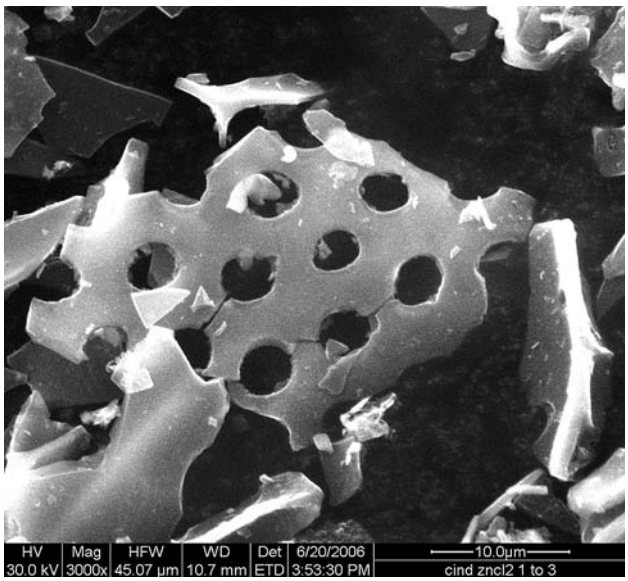

Fig. 12 SEM image of activated carbon from *Calotropis gigantia* activated with $ZnCl_2$ (wt/wt% ratio of Char:$ZnCl_2$ is 1:3; from ref. [23])

10 Preparation of Carbon Materials from *Calotropis gigantea* Stems Using Alkali Metal Carbonates as Activating Agent

The maximum values of specific surface area and pore volume values from $ZnCl_2$ activation of the stems of *Calotropis gigantea* are only 573 m^2/g and 0.29 cc/g. To attain further improvements in the textural parameters, the usefulness of alkali metal carbonates (Li_2CO_3, Na_2CO_3 and K_2CO_3) as chemical activating agents was examined. The char obtained by heating the dried stems of plant in a muffle furnace at 300 °C for 30 min was ground and sieved through a 200 mesh sieve to obtained fine carbon particles. It was next ground with the alkali carbonates in the desired proportion and activated at a temperature of 800 °C for 8 h in N_2 temperature.

10.1 Characterization of Carbon Materials Produced Using Alkali Metal Carbonates as Activating Agent

10.1.1 XRD Studies—Phase Structure of Carbon Material

XRD patterns of carbon materials were recorded using Shimadzu XD-D1 X-ray diffractometer operated at a scan range of 0.05° with CuKα radiation ($\lambda = 1.5418$ Å) and a Ni filter. The XRD pattern of the char comprises two broad diffraction peaks centered at 2θ values of 10 and 22°. The broad diffraction peak at a 2θ value of 22° is characteristic of the presence of lignin component [30, 31].

Above a 2θ value of 27° several sharp and intense diffraction peaks are observed in the XRD profile from the char and they are a result of silica and other typical mineral matter present in the plant tissues which remain intimately bound with carbon material in the char. Treatment of the char with NaOH (10 wt% solution) followed by HCl treatment (conc.) removed significant amount of mineral matter. The sharp diffraction peaks characteristic of such mineral matter were completely absent in the char sample produced after NaOH and HCl treatment. Significant changes in the XRD profiles were observed upon activation of the char with K_2CO_3. Upon activation, in addition to the retention of the inherent lignin structure, as evident from the retention of two broad peaks centered around 2θ values of 12 and 22°, a new diffraction peak originated at a 2θ value of 43.5 which is attributable to (10) diffraction of turbostratic carbon containing small hexagonal layer units of carbon. Similar observations are known in the literature [32, 33]. Beyond a char to K_2CO_3 ratio of 1:3, the intensity of the peak centered at 2θ value of 43.5 decreased steadily indicating the partial collapse of the turbostratic graphitic structure leading to a disordered carbon structure with hexagonal carbon layers misoriented to one another.

10.1.2 BET Sorptometry—Textural Properties of Carbon Materials

The sorptometric analysis on the char (as-synthesized material from *Calotropis gigantea*) as well as the activated carbon materials were carried out on Sorptometic 1990 Carbo Erba sorptometer using N_2 as adsorbent at 77 K (−196 °C). Prior to the analysis, the carbon samples were out gassed at 250 °C for 12 h. Details of the textural properties of the carbon materials are presented in Table 6. The specific surface area (SSA) is found to be maximum (1,296 m^2/g) at a K_2CO_3 to char ratio (wt/wt%) of 3 (Table 6). Thus, the optimum ratio of the activating agent to char is 3 (wt/wt%). At higher ratios, the SSA and the pore volume decreased.

The specific surface area of the activated carbon produced depends on the nature of the alkali cation, an increase in surface area of the carbon material is noticed with the radius of the cation of the activating agent (Table 7).

10.1.3 Effect of K_2CO_3 Activation on the Chemical Environment and the Concentration of Unpaired Electrons in Carbon from Calotropis gigantea

The EPR spectra of the char, char treated with base (NaOH) and acid (HCl) and the char activated with K_2CO_3 [char : K_2CO_3 = 1:3 (wt/wt)], shown in Fig. 13, were recorded on a Varian E-112, X band spectrometer at room

Table 6 Effect of amount of activating agent (K_2CO_3) on the specific surface area and pore volume values of carbon materials produced from *Calotropis gigantea*

S. no.	Sample	K_2CO_3:C (wt/wt%)	Specific surface area (m^2/g)	Specific pore volume (cm^3/g)
1	Char (as synthesised)	0	97	0.08
2	Activated Carbon1	1	892	0.50
3	Activated Carbon2	2	1,083	0.59
4	Activated Carbon3	3	1,296	0.73
5	Activated Carbon4	4	765	0.45
6	Activated Carbon5	5	922	0.53

Table 7 Effect of nature of cation of the activating agent (char to carbonate ratio = 1:1 wt) on the textural properties of activated carbon

S. no.	Activating agent	Ionic radii of the cation (Å)[a]	E^0 (V)[b,c]	Textural properties of carbon materials	
				Specific surface area (m^2/g)	Specific pore volume (cc/g)
1	Li_2CO_3	0.60	−3.0	480	0.263
2	Na_2CO_3	0.96	−2.7	811	0.395
3	K_2CO_3	1.33	−2.9	892	0.497

[a,b] From ref. [34, p. 197]

[b] $M + (\text{aq}) + e \rightleftharpoons M(s)$

[c] The standard redox potential of activated carbon is +0.24 V [35]

temperature using DPPH (diphenyl picryl hydrazyl) as the external reference to evaluate the g factor value and the spin concentrations.

The g-factor values, peak to peak separation, ΔH in Gauss, and the spin concentration values were evaluated and are summarized in Table 8. The spin concentration values were determined by following the procedure described in reference [36].

Important details from the data derived from the EPR spectra shown in Fig. 13 and summarized in Table 8 are:

1. the g factor values of the original char, char treated with base and acid as well as the char activated with K_2CO_3 are close to the *g* value of the free electron (2.002312) with in the error of our experiments (±0.002). Manivannan et al. [37], Vilas Ganpat Pol et al. [25], Singer and Wagoner [38], Chauvert et al. [39], Zhuo et al. [40] have made similar observations in the case of carbon materials produced from a variety of precursors.
2. the peak to peak separation was found to be higher in the case of the original char ($\Delta H = 11.0$ Gauss) compared to either the char treated with base and acid or the char activated with K_2CO_3. Such a broadness in the EPR signal is attributed to the presence of SiO_2 in the original char which was confirmed from XRD analysis. The decrease in ΔH value upon treatment with base and acid indicates the removal of the silica. As early as 1968, Singer and Wagoner [38] have made similar observation of broadening of the EPR signal resulting from graphite because of the presence of impurities like silica. Mrozowski has attributed the peak broadening to some changes in the structure of the carbon material [41]. Also from the data in Table 8, it is observed that upon activation with K_2CO_3 the ΔH value increased from 6.0 to 9.5 G indicating the presence of traces of K in the carbon material after activation leading to the slight broadening in the EPR signal.

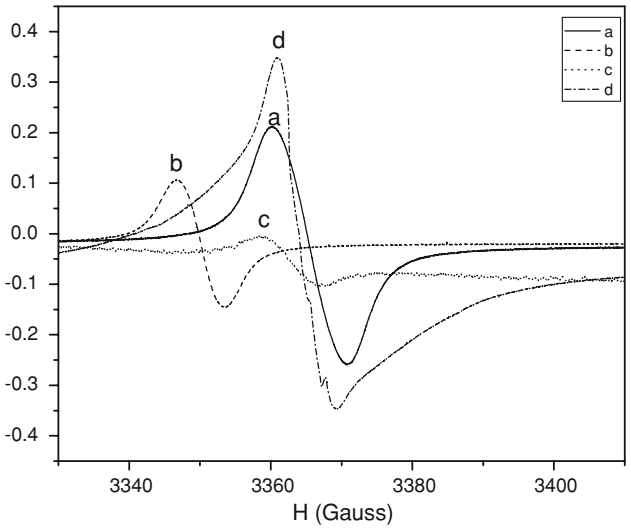

Fig. 13 EPR spectra of *a* char from *Calotropis gigantea*, *b* char treated with NaOH followed by HCl, *c* char activated with K2CO3 (char:K2CO3 (wt/wt%) = 1:3) and *d* DPPH

Table 8 The g-factor, peak-to-peak separation (ΔH in Gauss) and concentration of unpaired electrons in the carbon materials produced from *Calotropis gigantea*

Carbon material	*g*-Value	ΔH (in Gauss) peak to peak separation	Spin concentration/g of carbon
Char (as synthesized)	2.00092	11.0	0.73×10^{19}
Char (base and acid treated)	1.99980	6.0	0.33×10^{19}
Char activated with K_2CO_3 (char:K_2CO_3 = 1:3, wt/wt%)	2.00058	9.5	0.15×10^{16}

Table 9 Chemical composition of carbon materials from *Calotropis gigantea*

Element (wt%)	Carbon materials from *Calotropis gigantea*		
	Char (as synthesized)	Base and acid treated (NaOH and HCl) treated	Activated with K_2CO_3 (Char:K_2CO_3 = 1:3)
Carbon	73.13	77.62	80.04
Hydrogen	2.61	2.63	3.50
Nitrogen	0.81	0.82	0.67
Sulphur	0.36	0.33	0.36
Total	76.91	81.40	84.57
Ash content	12.7	4.0	1.8
Oxygen[a]	10.39	14.6	13.63

[a] By difference from the total amount of other constituents

3. The concentration of unpaired electrons in the char was found to be of the order of 0.74×10^{19}/g. The origin of such spins is attributed to the generation of dangling bonds formed as a result of the extensive devolatilization from the defragmentation of the hemicellulose, cellulose and lignin structure during the preparation of the char in the muffle furnace at 300 °C. Paramagnetic centers were found to be associated with the dangling bonds formed during the carbonization of carbon materials [42]. The spin concentration of the graphon black and acetylene black [43] were 1.1×10^{19} and 3.8 and 10^{19} spin/g, respectively which are of the same order of magnitude as that of the spin concentration value observed in the case of the unactivated char shown in Table 8.

Upon treatment of the char with base and acid, the spin concentration decreased from 0.74×10^{19} to 0.34×10^{19} spin/g. Nearly a three orders of magnitude reduction in the spin concentration is observed upon activation of char with K_2CO_3 (0.15×10^{16} spins/g). Such a drastic decrease in spin concentration upon activation with K_2CO_3 is because of the saturation of the dangling bonds with K metal, formed during the carbothermal reduction of K_2CO_3, resulting in the formation of surface C–K bonds which subsequently transform to C–H bonds upon final treatment with conc. HCl. Such a transformation is also confirmed from the increase in the hydrogen content (2.63–3.5 wt%) of the carbon sample activated with K_2CO_3 and subsequently treated with conc. HCl (Table 7). Manivannan et al. [37] have found the spin concentration values of activated carbon materials, namely, GX203 (from coconut

Table 10 Influence of the chemical activator on the textural properties of carbon materials

S. no.	Chemical activator	S_{BET} (m^2/g)	Pore volume (V_p) [cm^3/g]
1	Li_2CO_3	478	0.26
2	Na_2CO_3	811	0.40
3	K_2CO_3	892	0.50
4	$Ca(CO_3)_2$	524	0.33
5	$Ba(CO_3)_2$	170	0.10
6	$Zn(CO_3)_2$	626	0.30
7	NaCl	400	0.20
8	NaBr	319	0.16
9	KBr	275	0.10
10	NaI	58	0.04
11	CaO	521	0.25
12	$Ca(OH)_2$	189	0.11
13	$CaCl_2$	156	0.09
14	$Ba(OH)_2$	152	0.08
15	$Al(NO)_3$	253	0.19
16	Urea	439	0.21
17	Sodium acetate	548	0.26
18	Sodium oxalate	707	0.33
19	Sodium potassium tartarate	394	0.20
20	Sodium citrate	419	0.20
21	Sodium tartarate	394	0.20
22	Citric acid	127	0.07
23	Tartaric acid	42	0.04
24	Oxalic acid	317	0.14

The activation conditions are: carbon precursor:chemical activator (wt/wt%) ratio of 1:1, activation temperature of 800 °C, duration of activation is for 2 h

shell precursor), P1400 (from wood precursor) and Med50 (from coconut shell precursor) to be 1.8×10^{17}, 5.8×10^{17} and 1.8×10^{16} spins/g, respectively.

10.1.4 Elemental Analysis—Chemical Constitution of Carbon Materials

The elemental analysis of the char, char treated with NaOH followed by HCl and char activated with K_2CO_3 (char:K_2CO_3 (wt/wt%) = 1:3) was carried out in a CHNS/O analyzer (Perkin Elmer Instrument, Series II) and the results are presented in Table 9.

A simple treatment of the char with NaOH (10 wt% solution) and HCl in succession has improved the carbon content (wt%) from 73.13 to 77.62 which is attributed to the elimination of mineral matter. Activation with K_2CO_3 has further increased the carbon content from 77.62 to 80.04% and also the oxygen content decreased from 14.6 to 13.6% as expected. The increase in hydrogen (2.63–3.5 wt%) upon activation with K_2CO_3 is not because of activation step (reaction), but because of the subsequent treatment of the activated carbon composite (carbon material with the decomposed products of activated carbon, mainly K) with HCl and further washing with water. During the K_2CO_3 activation process surface species such as C–O–K are formed, which upon treatment with HCl and subsequent washing with water get transformed to C–O–H groups contributing to an increase in the hydrogen content in the case of activated carbon sample relative to either original char or the base and acid treated char.

11 Effect of the Nature of Activating Reagent on the Textural Properties of Activated Carbon Materials

The potential of various chemical compounds in tuning the textrual properties of carbon materials is summarized in Table 10. All the carbon materials exhibited Type I isotherms characteristic of microporous materials. It is observed that alkali salts of some carboxylic acids are as effective as alkali metal carbonates in improving the textural properties of carbon materials.

12 Catalytic Application of Carbon Materials for the Synthesis of Tert-Amyl Methyl Ether (TAME)

In the condensation reaction of tert-amyl alcohol (TAA) and methanol to form TAME, water is formed as a byproduct. The catalyst needs to be hydrophobic to resist the leaching of the active component. Carbon materials are sufficiently hydrophobic owing to the presence of graphite like chemical properties and can form an integral component of the catalyst. Acid function is the catalytic component needed to drive the etherification reaction. Heteropoly acids, particularly, dodeca tungstophosphoric (HPW) acid is a strong super acid with a H_0 value of −13.4 (more acidic than 100% sulphuric acid, $H_0 = -11.94$).

Four different carbon materials, namely, activated carbon from *Calotropis gigantea* (ACCG from K_2CO_3 activation), Black Pearl, Vulcan XC 72 R and CDX 975 with varying textural properties (Table 11) were employed as support material for HPW to evaluate the effect of the nature of carbon support on the activity of the supported solid acid catalyst. The HPW/C catalysts were prepared by impregnation-drying method using aqueous solutions of HPW. The carbon material and the HPW solutions were stirred at room temperature for 6 h followed by drying at 80 °C in a water bath to obtain 10 wt% HPW/C.

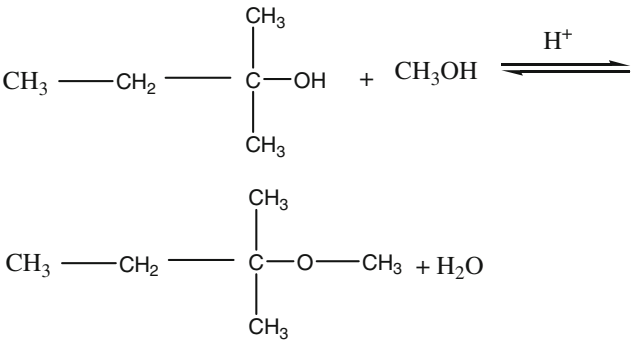

The catalytic activity of carbon supported heteropoly acids was investigated in the vapour phase synthesis of TAME as a test reaction. The reaction was carried out in a down flow fixed bed reactor at atmospheric pressure at a temperature of 373 K. The liquid feed containing tert-amyl alcohol (TAA) and methanol (in the mole ratio of 1:10) was fed onto the catalyst bed through a peristaltic pump (Miclins, SPO1) at a flow rate of 10 mL/h. N_2 was used as a carrier gas (flow rate, 30 mL/min). In a typical run, 0.5 g of the catalyst was charged in the reactor. The catalyst was stacked between glass beads and ceramic wool. The reactor was maintained under isothermal conditions during all runs. The reaction products were condensed at the bottom of the reactor and analyzed for the chemical composition using a gas chromatograph equipped with an OV 101 (packed) column and a FID detector.

The condensation reaction between tert-amyl alcohol and methanol over HPW/C catalysts was monitored for 3 h (Fig. 14). Reaction products were collected and analyzed

Table 11 Textural properties of the carbon materials and their catalytic activity after loading HPW (10 wt%) in the synthesis of TAME

Carbon material	S_{BET} (m^2/g)	Density (g/cc)	V_p (cc/g)	Conversion (wt%)[a]	Selectivity (%)	
					Olefins	TAME
CDX 975	215	0.23	0.28	75	35	65
Vulcan XC 72 R	224	0.33	0.46	54	13	87
Black Pearl 2000	1,012	0.15	1.15	7	47	53
Activated carbon—*Calotropis gigantea* (ACCG)	1,291	0.28	0.73	32	37	73

Reaction conditions: time on stream = 3 h; tert-amyl alcohol/methanol (mole) = 1:5; flow rate of the feed = 10 mL/h; flow rate of the carrier gas = 30 mL/min; amount of catalyst = 0.5 g

[a] Olefins: 2-methyl-2-butene (2MB2), 2-methyl-1-butene (2MB1)

by GC at intervals of 30 min. The catalytic activity was evaluated by monitoring the conversion of TAA with time. In situ generation of iso-amylenes (2-methyl-1-butene, 2MB1, and 2-methyl-2-butene, 2MB2) was observed during the course of the reaction. The formation of iso-amylenes is a result of the dehydration of the tert-amyl alcohol. The iso-amylenes formed subsequently react with MeOH to form TAME. Details of conversion (wt%) of TAA and selectivity towards olefins and TAME over different HPW/C catalyst are summarized in Table 11. The results reveal that the activity and selectivity are not apparently related to the surface areas of the carbon supports. Activity for the etherification could be related to many factors, such as the dispersion of HPW, the distribution of HPW in the pores, the accessibility of the active sites (through diffusion) to the reactants and the presence/absence of poisons on the surface of the support. All the catalysts tend to deactivate slowly with duration of run, the more active catalyst (CDX 975) deactivating faster than the other (Fig. 14).

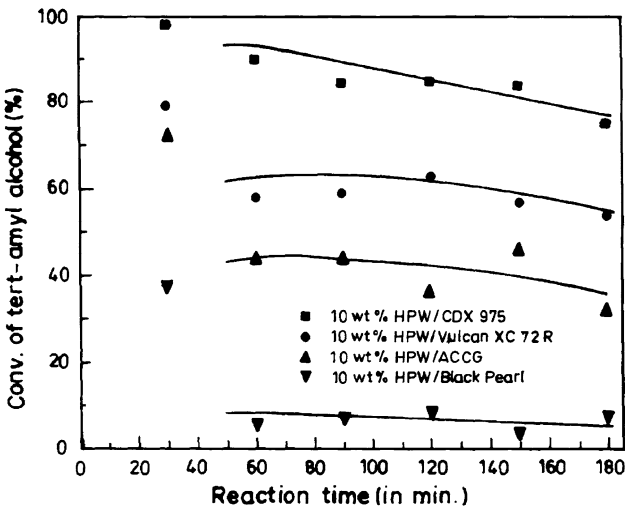

Fig. 14 Plot of conversion of TAA (wt%) versus reaction time (in minutes)

13 Carbon Materials (as Adsorbents) for Adsorptive Desulphurization

13.1 Studies on Neat Carbon Samples

Removal of organo-sulphur compounds from diesel is an issue of interest from scientific, social, economic and environmental view points. Production of clean fuel is the goal of petroleum refining industry. The reduction of S below certain levels in diesel fuels becomes difficult due to the presence of sterically hindered S-compounds (such as the 4,6-dialkydibenzothiophenes) that are difficult to desulfurize over conventional supported mixed sulfide catalysts. Hence, newer technologies based on novel routes like adsorption, oxidation and chelation are being developed to remove these refractory S-compounds. We now summarize in the following section our work on the use of carbon materials for the adsorptive desulfurization of a medium S-containing straight run diesel fraction with a S content of 737 ppm, from Cauvery Basin Refinery (CBR), India.

The physicochemical properties of the CBR diesel are summarized in Table 12. Several commercially available activated carbon materials of varying physical and chemical properties were tested as adsorbents for the removal of organo sulphur compounds from CBR diesel. The carbon materials used were adsorbent carbon (A) from Adsorbent Carbons Pvt. Ltd., India. Calgon carbon (B) from Calgon Carbon (Tianjin) Co. Ltd., Activated carbons, IG 18 × 40, IG 12 × 40 and IG 8 × 30 from Indo-German Carbon Ltd., India and the Activated carbons, AC 4 × 8, AC 6 × 12, AC 12 × 30 from Active Carbon Pvt. Ltd., India.

In a typical adsorption experiment, a glass column of length 50 cm and internal diameter 1.5 cm was packed with 5.0 g of carbon sorbent with glass beads on either

Table 12 Properties of SR diesel from CBR distillation unit used in the studies

Property	Value
Total sulphur content (in ppm)	737
Flash point (°C)	93
Aniline point (°C)	81
Viscosity (at 40°C in cSt)	4.04
Pour point (°C)	+6
Density (g/cc)	0.8553
Diesel index	60
Cetane index	53

side. Diesel was fed on top of the sorbent bed. The first 20 mL product collected at the out let was analyzed for S. From the S content remaining in the product and subtracting the same from the S content in the feed diesel (737 ppm), the S removed by the carbon was obtained. The S content in the product was analyzed by using an Oxford XRF analyzer. The feed and the product diesel were also analyzed (in some experiments) for individual sulphur compounds using a GC-PFPD (Gas Chromatography–Pulsed Flame Photometric Detector).

Different commercially available activated carbons, namely, IG 18 × 40, IG 12 × 10, IG 8 × 30, AC 4 × 8, AC 6 × 12, Ac 12 × 30, calgon carbon as received and adsorbent carbon as received were used as adsorbents for S containing compounds present in SR diesel. The results obtained on the studies with the afore mentioned adsorbents are given in Table 13. The amount of S removed (in ppm) from 20 mL deisel by 5.0 g of sorbent is shown in extreme right column of Table 13. Among the eight carbons studied adsorbent carbon as received and calgon carbon as received were superior to the others for the adsorption of S-compounds in diesel. Hence, adsorbent carbon (A) and calgon carbon (B) were selected for subsequent studies.

Table 13 S removal capacity of different commercial activated carbon materials

Activated carbon as sorbent	mL-diesel treated/g of adsorbent[a]	S removed (ppm)
IG 18 × 40	4	134
IG 12 × 10	4	81
IG 8 × 30	4	76
AC 4 × 8	4	12
AC 6 × 12	4	73
AC 12 × 30	4	92
Calgon carbon as received	4	181
Adsorbent carbon	4	229

[a] A 20 mL initial product collected from the column packed with 5.0 g activated carbon and analyzed for S

13.2 Studies on Activated Carbon Samples [Adsorbent Carbon (A) and Calgon Carbon (B)]

13.2.1 Activation with Conc. HNO_3

HNO_3 treatment changes the surface chemistry of carbon materials. Such oxidative treatment results in the formation of oxygen containing surface functional groups (carbonyl and carboxyl). The presence of such surface functional groups, in most cases, enhances the adsorption capacity of carbon materials [44, 45]. Two commercial activated carbon materials, namely, the adsorbent carbon (A) and the calgon carbon (B) were treated with conc. HNO_3. The wt/wt% ratio of carbon to conc. HNO_3 was 1:5. The oxidative treatment of carbon with conc. HNO_3 was carried out at 60 °C for 2 h under refluxing conditions in a 2-L RB flask. The contents were then cooled to room temperature, washed with water and dried at 110 °C for 2 h.

13.2.2 Activation Under Ar Atmosphere

Ar activation involved the thermal activation of nitric acid treated carbon materials A and B at a temperature of 800 °C under Ar atmosphere for 2 h in a quartz tube. The carbon samples after activation were termed as nitric acid treated Ar activated carbon materials.

13.3 Characterization of Adsorbents for Desulphurization Application

13.3.1 XRD Analysis

X-ray diffraction patterns of adsorbent carbon as received, adsorbent carbon treated with conc. HNO_3 and adsorbent carbon treated with HNO_3 followed by subsequent activation in Ar atmosphere are shown in Fig. 15A(a–c), respectively. Two broad diffraction peaks centered at 2θ values of 25.4 and 43.4 are observed in all the patterns. These peaks can be indexed, respectively, to (002) and (101) planes of crystalline hexagonal graphite lattice [(JCPDS-41-1487), 46].

The phase structure of adsorbent carbon remained unaltered upon nitric acid treatment [Fig. 15A(a, b)]. But in the case of adsorbent carbon treated with nitric acid followed by activation in Ar atmosphere an additional intense and narrow diffraction peak is seen at $2\theta = 26.7$ [Fig. 15A(c)]. This is attributed to (002) reflection from highly crystalline graphitic carbon [47]. Nitric acid treated Ar activated adsorbent carbon [Fig. 15A(c)] is more crystalline than either adsorbent carbon as received or adsorbent carbon treated with nitric acid alone. Thus Ar activation improved the crystallinity of nitric acid treated adsorbent carbon.

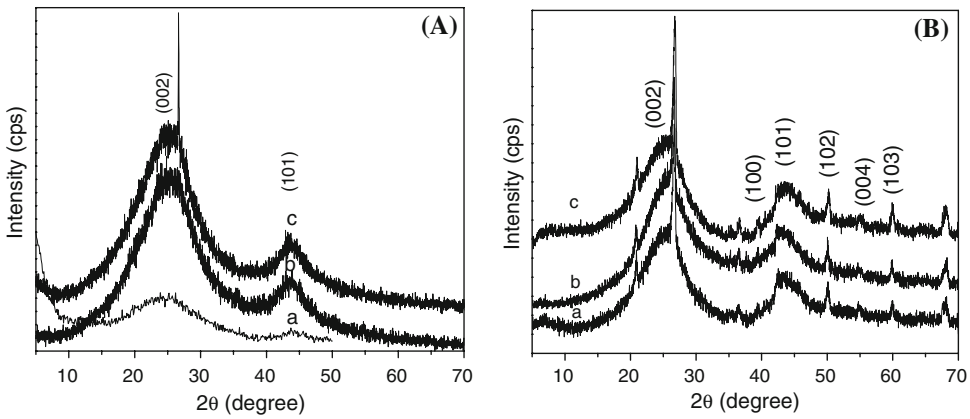

Fig. 15 XRD patterns of **A**: *a* adsorbent carbon as received, *b* adsorbent carbon treated with HNO_3 and *c* adsorbent carbon treated with HNO_3 and activated with Ar; **B**: *a* calgon carbon as received, *b* calgon carbon treated with HNO_3 and *c* calgon carbon treated with HNO_3 followed by Ar activation

X-ray diffraction patterns of calgon carbon as received, calgon carbon treated with HNO_3 and calgon carbon treated with HNO_3 followed by Ar activation are shown in Fig. 15B(a–c), respectively. The diffraction peaks arising from each of these carbon samples were indexed and are typical of graphitic carbon structure [47]. Neither HNO_3 treatment [Fig. 15B(b)] nor HNO_3 treatment with subsequent Ar activation [Fig. 15B(c)] significantly altered the structure of the original calgon carbon sample [Fig. 15B(a)]. Thus, neither HNO_3 treatment nor Ar activation has much influence on the phase structure of calgon carbon.

There is a marked difference in the structural order between adsorbent carbon and calgon carbon. No diffraction peaks resulted from adsorbent carbon or its modified forms beyond $2\theta = 50^{\circ}$ (Fig. 15A) in sharp contrast to the characteristic diffraction peaks resulting from Calgon and modified calgon carbon above $2\theta = 50^{\circ}$ (Fig. 15B) Thus, calgon carbon appears to be structurally more ordered than adsorbent carbon.

13.3.2 BET Sorptometric Studies

The N_2 adsorption-desorption isotherms (not shown) of the different treated adsorbent carbons were typically of the type I (characteristic of microporous materials) while those of the Calgon based samples were slightly different in that some multilayer adsorption was also noticed suggesting the presence of larger (meso) pores. The surface area and pore volumes of the different samples are presented in Table 14.

13.3.3 FT-IR Studies

The FT-IR spectra of adsorbent carbon and calgon carbon, as received, treated with HNO_3 and treated with HNO_3 followed by Ar activation are presented in Fig. 16A, B.

The main distinguishing feature observed in the Activated carbon samples after nitric acid treatment is the

Table 14 Surface area and pores volumes of adsorbent carbon, calgon carbon and their modified forms

Carbon	Specific surface area (m^2/g)	Total pore volume (cm^3/g)
Adsorbent carbon as received	950	0.451
Adsorbent carbon treated with Conc. HNO_3	882	0.398
Adsorbent carbon treated with Conc. HNO_3 followed by Ar activation	1,048	0.523
Calgon carbon as received	1,014	0.587
Calgon carbon treated with Conc. HNO_3	649	0.387
Calgon carbon treated with Conc. HNO_3 followed by Ar activation	996	0.598

generation of a shoulder at 1,749 cm^{-1} [Fig. 16A(b)] attributed to the stretching vibration of C=O bond (aldehydes, ketones, lactones or carboxyl groups). This shoulder at 1,749 cm^{-1} becomes intense and develops into a sharp peak upon activation in Ar atmosphere [Fig. 16A(c); 48, 49]. But for this difference all the three samples showed similar but rich surface chemistry with a variety of oxygen containing functional groups. A number of functional groups are common to adsorbent carbon and its modified forms [Fig. 16A(a–c)]. These are: a sharp band at 3,738 cm^{-1} is ascribed to isolated OH groups, a broad, intense band in the range of 3,200–3,600 cm^{-1} with a maximum at about 3,440 cm^{-1} assigned to the O–H stretching mode of hydroxyl groups and adsorbed water [50], two sharp, narrow and intense bands at 2,922 and 2,855 cm^{-1} as a result of, respectively, the asymmetric and symmetric C–H stretching vibrations of the methylene group [51–53], a sharp intense peak at 1,640 cm^{-1} attributed to the carbonyl groups in quinone, broad bands observed in the range of 1,300–1,000 cm^{-1} attributed to C–O stretching in acids, alcohols, phenols, ethers and esters and lastly, broad bands in the range of

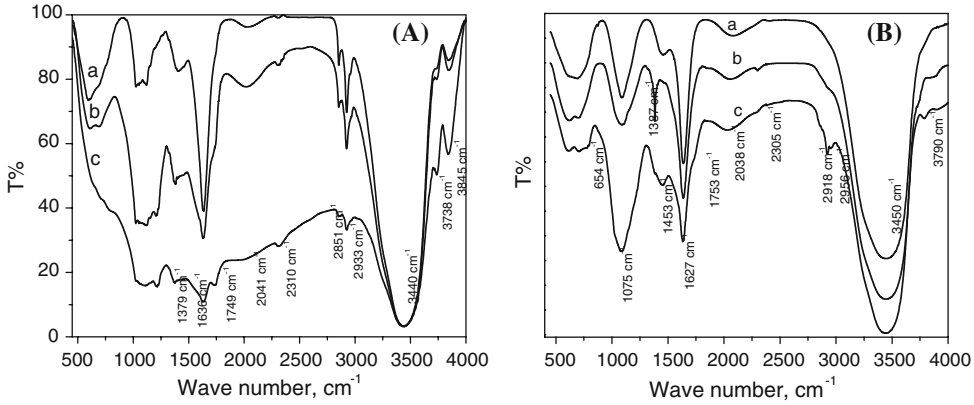

Fig. 16 FT-IR spectra of **A**: *a* adsorbent carbon as received, *b* adsorbent carbon treated with HNO_3 and *c* adsorbent carbon treated with HNO_3 and activated with Ar; **B**: *a* calgon carbon as received, *b* calgon carbon treated with HNO_3 and *c* calgon carbon treated with HNO_3 followed by Ar activation

Table 15 S sorption capacity of the different carbon samples

Carbon	S removed[a] (in ppm)
Adsorbent carbon as received	410
Adsorbent carbon treated with HNO_3	577
Adsorbent carbon treated with HNO_3 followed by Ar activation	586
Calgon carbon as received	451
Calgon carbon treated with HNO_3	488
Calgon carbon treated with HNO_3 followed by Ar activation	619

[a] S removed from the first 20 mL diesel after passing through the sorbent bed; S content in the diesel feed—737 ppm; Carbon loading: 15 g

Table 16 Type and amount of the S compounds in the feed and the product diesel (after passing through the carbon bed) as analyzed by GC-PFPD [55]

Sulphur species[a]	S content (in ppm)		
	CBR diesel (feed)	Adsorbent carbon HNO_3 followed by Ar treatment, 15.0 g	Calgon carbon, HNO_3 followed by Ar treatment, 15.0 g
C_1BT	4.6	Nil	Nil
C_2BT	119.6	Nil	Nil
C_3BT	137.5	75.2	67.2
C_3^+BT	79.6	68.9	47.4
DBT	91.5	2.6	1.3
C_1DBT	157.7	Nil	Nil
C_2DBT	116.7	Nil	Nil
C_3DBT	29.5	4.3	2.1
Total S	737	151	118

[a] C_1, C_2, C_3, C_3^+ BT and DBT—mono, di, tri and multi alkyl substituted benzothiophene and dibenzothiophenes

600–800 cm^{-1} as a result of the out of plane deformation mode of C–H in various substituted benzene rings [50, 51].

In the case of the calgon carbon samples (Fig. 16B), activation with conc. HNO_3 creates new bands at 3,790, 2,305 and 1,387 cm^{-1} attributable to isolated O–H groups, ketone surface groups [54] and the in-plane bending vibration of C–H in methyl group [28], respectively [Fig. 16B(b)]. In addition to the generation of –OH, C=O and $–CH_3$ groups, a broad featureless shoulder is observed in the range 2,910–2,990 cm^{-1}, due to aliphatic C–H stretching in methylene and methyl groups.

Ar activation of Conc. HNO_3 treated calgon carbon induces certain specific changes into the spectral features. The first and foremost change is the appearance of a broad shoulder at 1,753 cm^{-1} attributable to the C=O group of carboxylic acid groups Fig. 16B(c). Also, the broad featureless shoulder present in the HNO_3 treated calgon carbon (in the range 2,910–2,990 cm^{-1}) develops into two clear sharp peaks centered at 2,956 and 2,918 cm^{-1}, which are attributed to the asymmetric and symmetric stretching vibrations of C–H in methylene groups indicating the generation of hydrophobic methylene C–H groups on the surface of calgon carbon on activation with Ar. In spite of the several striking changes brought about, as discussed above, into the surface functionality of calgon carbon upon treatment with conc. HNO_3 and subsequent Ar activation, some inherent functional groups of parent calgon carbon remained unaltered even after modification. The spectral features common to all the three samples [Fig. 16B(a–c)] are as follows: a broad intense transmission peak centered at 3,450 cm^{-1} corresponding to OH stretching mode of hydroxyl groups and adsorbed water and a broad intense peak centered at 1,075 cm^{-1}, which can be attributed to C–O stretching in acids, alcohols, phenols, ethers and esters [52].

13.4 Evaluation of the Adsorptive Desulphurization Potential of Adsorbent and Calgon Based Carbon Materials

The results of the adsorptive desulphurization experiments are presented in Table 15. Both nitric acid treatment and subsequent Ar activation enhanced the S adsorption ability of the carbon samples, the Ar activated samples being more

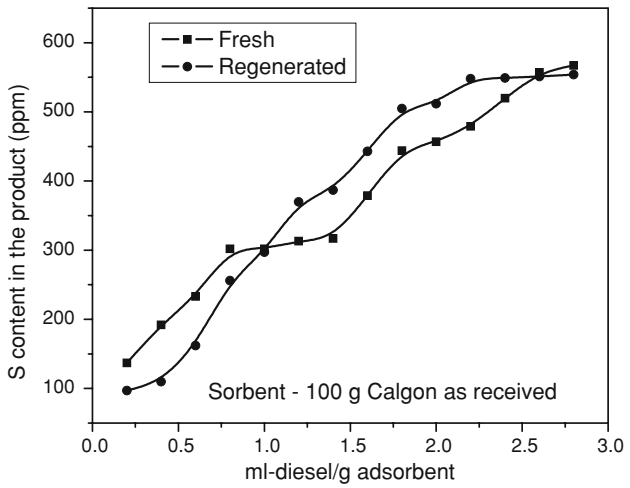

Fig. 17 Plot of S removal capacity of fresh versus toluene regenerated sorbent (100 g calgon carbon used as received)

active for adsorption. Combination of nitric acid treatment and Ar activation induces suitable surface functionality, polarity (surface hydrophilic and hydrophobic functional groups), phase structure (discussed under XRD) and pore structure into the carbon adsorbents facilitating enhanced adsorption of the organo-sulphur compounds present in the diesel feed stocks.

The nature of the S components present in the product diesel was analyzed using GC-PFPD and the results obtained over 15.0 g sorbent bed using modified adsorbent carbon (A) and calgon carbon (B) are shown in Table 16. It is observed that the most highly refractive compounds (C_2BT and C_2DBT) present in the feed prior to desulphurization process are absent in the product diesel after the adsorption process exemplifying the utility and usefulness of the process in selectively adsorbing the refractory S-compounds that are difficult to desulfurize over conventional hydrotreating catalysts.

The carbon samples after S-adsorption could be regenerated by washing with toluene (500 mL for 100 g spent carbon) at room temperature followed by drying the sorbent bed at 110 °C. The results of the adsorption experiments over neat and solvent regenerated calgon carbon (without modification) are shown in Fig. 17. It is evident from the adsorption plots that the regenerated sorbents performance is on a par with that of the fresh calgon carbon as received. Thus an efficient and environmentally benign regeneration method and a process for the adsorptive desulfurization appear to be feasible based on carbon materials.

14 Conclusions

The development of carbon materials has always been a challenging problem from the point of view of their source and activation procedures to create characteristics necessary to exploit them for various applications, including as support for noble metals (used in electrodes and as catalysts for organic transformations) and adsorption purposes. We have reported the use of natural raw materials for developing carbon materials useful in fuel cell electrode applications. We have also demonstrated the use of appropriate activation treatments to modify the textural and surface functionalities at the surface of carbon materials. The possibility of employing these developed carbon materials or carbon materials available from other sources in some applications as supports for electro-catalysts and for specific applications like adsorptive desulphurization has been investigated.

Acknowledgments The authors wish to record their gratefulness to the Department of Science and Technology, India, The Chennai Petroleum Corporation Limited (CPCL) and Ms. Columbian Chemicals Company, USA, for supporting the work.

References

1. Viswanathan B, Indra Neel P, Varadarajan T K (2009) Methods of activation and specific applications of carbon materials, E-book, http://nccr.iitm.ac.in
2. Viswanathan B, Aulice Scibioh M (2006) Fuel cells: principles and applications, Universities Press
3. Ren B, Li XQ, She CX, Wu DY, Tian ZQ (2000) Electrochim Acta 46:193
4. Carabineiro SAC, David Thompson T (2007) Catalytic applications of gold nanotechnology in nanoscience and technology, nanocatalysis. In: Heiz U, Landman U (eds) Springer, Berlin, p 463
5. Andrew Dicks L (2006) J Power Sources 156:128
6. Rajesh B (2002) Methanol oxidation anodes based on conducting polymers and carbon nanotubes supported noble metal (s) for possible applications in DMFC, Ph. D. thesis, Indian Institute of Technology Madras
7. Samant PV, Rangel CM, Romero MH, Fernandes JB, Figueiredo JL (2005) J Power Sources 151:79
8. Viswanathan B (2009) Catal Today 141:52
9. Mohindar Seehra S, Arthur Pavlovic S (1993) Carbon 31:557
10. Suresh Babu V, Seehra MS (1996) Carbon 34:1259
11. West AR (1984) Solid State Chemistry and its Applications. Wiley, Chichester, p 734
12. Liu Z, Ling XY, Su X, Lee JY (2004) J Phys Chem B 108:8234
13. Manohara R, Goodenough JB (1992) J Mater Chem 2:875
14. Liu Z, Lee JY, Chen W, Han M, Gan LM (2004) Langmuir 20:181
15. Sevilla M, Sanches C, Valdos-Sols T, Moralln E, Fuertes AB (2007) J Phys Chem C 111:9749
16. Niu JJ, Wang JN, Zhang L, Shi Y (2007) J Phys Chem C 111:10329
17. Lei Z, Bai S, Xiao Y, Dang L, Au L, Zhang G, Xu Q (2008) J Phys Chem C 111:722
18. Zheng S-F, Hu J-s, Zhong LS, Wan LJ, Song WG (2007) J Phys Chem C 111:11174
19. Sobkowski J, Franaszczuk K, Dobrowolska K (1992) J Electroanal Chem 330:529
20. Wu G, Xu B-Q (2007) J Power Sources 174:148

21. Liu Z, Lee JY, Chen W, Han M, Gan LM (2004) Langmuir 20:181
22. Lin M-L, Huang C-C, Lo M-Y, Mou C-Y (2008) J Phys Chem C 112:867
23. Indra Neel P (2009) Methods of activation and specific applications of carbon materials from natural sources, Ph. D. thesis, Indian Institute of Technology Madras
24. Prahas Devarly, Kartika Y, Indraswati N, Ismadji S (2008) Chem Eng J 140:32
25. Pol VG, Motiei M, Gedanken A, Calderon-Moreno J, Yoshimura M (2004) Carbon 42:111
26. Ruland W (1990) Adv Mater 2:528
27. Ruland W, Smarsly B (2002) J Appl Crystallogr 35:624
28. Yang T, Lua AC (2006) Mater Chem Phys 100:438
29. Lespade P, Al-Jishi R, Dresselhaus MS (1982) Carbon 20:427
30. Rials TG, Glasser WG (1989) J Appl Polym Sci 37:2399
31. Sarkar S, Adhikari B (2001) Eur Polym J 37:1391
32. Kubo S, Uraki Y, Sano Y (2003) J Wood Sci 49:188
33. Sricharoenchaikul V, Pechyen C, Aht-ong D, Atong D (2008) Energy Fuels 22:31
34. Cotton FA, Wilkinson G (1976) Basic inorganic chemistry. Wiley, New York
35. Adams MD (1991) Hydrometallurgy 26:201
36. Sarathi R, Rajesh Kumar P, Sahu RH (2007) Polym Degrad Stab 92:560
37. Manivannan A, Chirila M, Giles NC, Seehra MC (1999) Carbon 37:1741
38. Singer LS, Wagoner G (1968) Carbon 6:199
39. Chauvert O, Forro L (1995) Phys Rev B Condens Mater 52:R6963
40. Zhuo O, Fleming RM, Murphy DW, Chen CH, Haddon RC, Ramirez AP, Gharum SH (1994) Science 263:1744
41. Mrozowski S (1979) Carbon 17:227
42. Freitas JCC, Bonagamba J, Emmerich FG (2001) Carbon 39:535
43. Donnet JB, Bansal R, Wang M-J (1993) Carbon black—science and technology, 2nd edn. Revised and expanded. CRC publications
44. Joong Noh S, James Schwarz A (1990) Carbon 28:675
45. Gomez-Serrano V, Acedo-Ramos M, Lopez-Peinado AJ, Valenzuela-Calahorro C (1997) Thermochim Acta 291:109
46. Shao M, Wang D, Yu G, Hu B, Yu W, Qian Y (2004) Carbon 42:183
47. Macia-Agullo JA, Moore BC, Cazoria-Amoros D, Linares-Solana A (2007) Microporous Mater 101:397
48. Budinova T, Ekinci E, Yardim F, Grimm A, Bjornbom E, Minkova V, Goranova M (2006) Fuel Process Techonol 87:899
49. Ishizaki C, Marti I (1981) Carbon 19:409
50. Madhava Rao M, Ramesh A, Purna Chandra Rao G, Seshaiah K (2006) J Hazard Mater B129:123
51. Puziy AM, Poddubnaya OI, Martinez-Alonso A, Suarez-Garcia F, Tascon JMD (2003) Carbon 41:1181
52. Alexander Puziy AM, Olga Poddubnaya I, Alonso AM, Garcia FS, Jaun Tascon MD (2005) Carbon 43:2857
53. Gercel O, Ozcan A, Safa Ozcan A, Ferdi Gercel H (2007) Appl Surf Sci 253:4843
54. Macias-Garcia A, Diaz-Diez MA, Cuerda-Correa EM, Olivares-Marin M, Ganan-Gomez J (2006) Appl Surf Sci 252:5972
55. Selvavathi V, Meenakshisundaram A, Sairam B, Indra Neel P, Rajasekaran M, Viswanathan B (2008) Adsorptive desulphurization of diesel by modified carbons. In: 6th international symposium on fuels and lubricants (ISFL-2008), March 9–12, 2008 at New Delhi